Chinese Journal of
POLYMER SCIENCE

RESEARCH ARTICLE

https://doi.org/10.1007/s10118-022-2819-9
Chinese J. Polym. Sci. **2022**, *40*, 1594–1603

ZnO Surface Passivation with Glucose Enables Simultaneously Improving Efficiency and Stability of Inverted Polymer: Non-fullerene Solar Cells

Bo-Wen Liu[a,b], Ze-Rui Li[b], Ling-Peng Yan[b], Jing-Bo Guo[b], Qun Luo[a,b], and Chang-Qi Ma[a,b*]

[a] *School of Nano-Tech and Nano-Bionics, University of Science and Technology of China, Hefei 230026, China*
[b] *i-Lab & Printable Electronics Research Center, Suzhou Institute of Nano-Tech and Nano-Bionics, Chinese Academy of Sciences, Suzhou 215123, China*

Electronic Supplementary Information

Abstract The power conversion efficiency (PCE) of polymer solar cells (PSCs) has exceeded 19% due to the rapid progress of photoactive organic materials, including conjugated polymer donors and the matched non-fullerene acceptors (NFAs). Due to the high density of oxygen vacancies and the consequent photocatalytic reactivity of ZnO, structure inverted polymer solar cells with the ZnO electron transport layer (ETL) usually suffer poor device photostability. In this work, the eco-friendly glucose (Glu) is found to simultaneously improve the efficiency and stability of polymer:NFA solar cells. Under the optimal conditions, we achieved improved PCEs from 14.77% to 15.86% for the PM6:Y6 solar cells. Such a PCE improvement was attributed to the improvement in J_{SC} and FF, which is ascribed to the smoother and more hydrophobic surface of the ZnO/Glu surface, thereby enhancing the charge extraction efficiency and inhibiting charge recombination. Besides, UV-Vis absorption spectra analysis revealed that glucose modification could significantly inhibit the photodegradation of Y6, resulting in a significant improvement in the stability of the device with 92% of its initial PCE after aging for 1250 h. The application of natural interface materials in this work brings hope for the commercial application of organic solar cells and provides new ideas for developing new interface materials.

Keywords Polymer solar cells; Glucose; Surface passivation; Charge injection; Stability improvement

Citation: Liu, B. W.; Li, Z. R.; Yan, L. P.; Guo, J. B.; Luo, Q.; Ma, C. Q. ZnO surface passivation with glucose enables simultaneously improving efficiency and stability of inverted polymer:non-fullerene solar cells. *Chinese J. Polym. Sci.* **2022**, *40*, 1594–1603.

INTRODUCTION

Polymer solar cells (PSCs) are expected to become a new generation of photovoltaic technology owing to their flexibility,[1] lightweight and solution processability.[2,3] The power conversion efficiency (PCE) of PSCs has exceeded 19%[4] due to the rapid progress of the photoactive materials, including wide bandgap conjugated polymer donors[5,6] and the matched non-fullerene acceptors (NFAs).[7–10] Especially with the emergence of the star molecules PM6[11] and Y6,[12] the PCE of the PSC has started a rapid improvement.[13,14] The high-efficiency organic solar cells are composed of a transparent conductive electrode, the photoactive layer, and a metal electrode.[15] Generally, the hole and electron transport layers (HTL and ETL) are used to obtain a better ohmic contact with the corresponding electrodes.[16,17] Zinc oxide (ZnO), as a low work function metal oxide, is the most popular ETL in PSCs[18–20] owing to its solution processibility, excellent electron mobility, and medical compatibility. However, due to the high density of oxygen vacancies as electronic traps,[21,22] surface charge recombination as well as "light-soaking" effect inevitably occur in ZnO-based PSCs, leading to low PCEs.[23,24] Besides, the defect states on the surface of ZnO can induce the photocatalytic degradation of the NFAs, leading to the rapid PCE decay of the cells.[22,25,26] Therefore, surface modification of ZnO layer is critical for non-fullerene solar cells. Over the last few years, various organic ligands that can coordinate to Zn^{2+}, such as ethanedithiol (EDT),[27] polyethylenimine (PEI),[25] as well as Lewis acid,[28] were used as the surface modification layer to improve the performance and stability of PSCs. Even though the device performance was successfully improved, most of the above-mentioned surface modifiers are industrial chemical products with potential environmental hazards. An environment-friendly organic ligand that can effectively passivate the surface defects of ZnO is therefore highly interesting to the PSC technology.

As a bio-activate small molecule, glucose (Glu) is the main product of photosynthesis and exists widely in nature. In addition, the glucose molecule has several hydroxyl groups that potentially can coordinate to Zn^{2+}. Therefore, glucose is a green chemical with low cost and biocompatibility advantages, making it highly suitable as a surface modifier of ZnO

* Corresponding author, E-mail: cqma2011@sinano.ac.cn

Invited Research Article for Special Issue on "Organic Photovoltaic Polymers"
Received April 2, 2022; Accepted June 1, 2022; Published online September 21, 2022

layer in PSC. Lin *et al.* reported using glucose-based polymers, including chitosan, methylcellulose, and dextrin, as the ZnO surface modifier in inverted PSC, where improved device performance was achieved.[29] Except for this, no other research on the use of glucose in polymer solar cells was reported. Herein, we report the application of glucose as ZnO surface modifier in inverted PSC. We found that the device based on ZnO/Glu ETL exhibits an increased short-circuit current density (J_{SC}) and fill factor (FF), and the ultimate higher power conversion efficiency was measured for the Glu-cooperated cells when compared to the Glu-free reference cells. Most importantly, the Glu-based cells also showed improved performance stability in comparison with the Glu-free reference cells. The performance and stability improvement of the glucose passivation effect was investigated.

EXPERIMENTAL

Materials

PM6 (PBDB-T-2F) and IT-4F, Y6 and N3 were purchased from Solarmer Materials Inc, Beijing. $Zn(OAc)_2$, TMAH, and glucose (Glu) were purchased from J&K Scientific Ltd. 1,8-Diiodooctane (DIO) and 1-chloronaphthalene (CN) were purchased from Sigma-Aldrich. Molybdenum(VI) oxide (MoO_3) was purchased from Strem Chemicals. All materials were used as received without further purification. ZnO was prepared through the reaction between TMAH and $Zn(OAc)_2$ in DMSO as reported by Qian *et al.*[30]

Instruments and Measurement

The ultraviolet-visible (UV-Vis) absorption and transmittance spectra of ZnO and NFAs films were measured with a PerkinElmer Lambada 750 at room temperature. All the films were spin-coated on the glass substrates and aged in glove box under white LED light. ZnO were spin-coated on the ITO substrates and then were annealed on a hot plate in glove box. Then Glu was also spin-coated on the ZnO and was annealed. The surface roughness of the samples was analyzed by atomic force microscopy (AFM) with a probe-type Park XE-120 microscope. The samples were put into a N_2-filled chamber and transferred to the vacuum chamber for XPS testing as careful as possible to minimize the undesired contamination.

Fabrication of Polymer Solar Cells

ITO substrates were sequentially cleaned by detergent, deionized water, acetone, and isopropanol in ultrasound cleaner. Before using them, they were firstly dried by N_2 flow and then treated in a UV-ozone oven for 30 min. First, ZnO NPs (10 mg/mL in ethanol) was spin-coated on the ITO substrates at 2000 r/min for 60 s and then were annealed at 130 ℃ for 10 min. Then, the Glu (0.5mg/mL in methanol) was spin-coated on the top of the ZnO electron transportation layer at 3000 r/min for 30 s and then were annealed at 130 ℃ for 5 min on a hot plate in glove box filled with N_2. The mixed solution of PM6:Y6 (N3) together with 0.5 vol% CN was dissolved in chloroform (CF) with concentrations of 7 and 8.4 mg/mL, respectively. The solution of PM6:IT-4F (10 mg/mL for each compound) blended in chlorobenzene (CB) with 0.5 vol% DIO was spin-coated on the top of the ZnO electron transportation layer at 2000 r/min for 60 s and then were annealed at 130 ℃ for 10 min on a hot plate in glove box filled with N_2. Finally, MoO_3 (20 nm) as the hole-extraction layer and Al (100 nm) as the anode were sequentially vacuum deposited on the top of the active layer respectively. The effective photovoltaic area, defined by the geometrical overlap between the bottom cathode electrode and the top anode, was 0.09 cm^2.

PV Parameters of Polymer Solar Cells

The PV parameters of the cells including open-circuit voltage (V_{OC}), J_{SC} and FF were measured using a Keithley 2400 source meter under illumination with simulated AM 1.5G sunlight (Zolix, Sirius-SS150A) in a glove box filled with N_2. The external quantum efficiency (EQE) spectra were recorded by EQE system which was built in home and the light from a 150 W tungsten halogen lamp (Osram 64610) was used as a probe light and was modulated with a mechanical chopper before passing through the monochromator (Zolix, Omni-k300) to select the wavelength. The response was recorded as the voltage by an *I-V* converter (D&R-IV Converter, Suzhou D&R Instruments), using a lock-in amplifier (Stanford Research Systems SR 830). With a stand silicon cell as the reference before testing the devices.

Degradation of Polymer Solar Cells under White Light

The long-term stability of un-encapsulated devices was conducted by multi-channel solar cell performance decay test system (PVLT-G8001M, Suzhou D&R Instruments Co., Ltd.) under a testing condition in accordance with ISOS-L-1 in the glove box. The cells were put inside a glove box filled with N_2 (H_2O<10 ppm, O_2<10 ppm) and continuously illuminated with white LED light (D&R Light, L-W5300KA-150, Suzhou D&R Instruments). The illumination light intensity was initially set so the output J_{SC} is as same as that measured under standard conditions by AM1.5G. For monitoring changes in illumination light intensity, it was monitored by a photodiode (Hamamtsu S1336-8BQ). *J-V* characters of the devices were checked periodically, and the photovoltaic performances data (V_{OC}, J_{SC}, FF and PCE) were calculated automatically according to the *J-V* curves. When *J-V* was tested, an external load matching the maximum power output point ($R_{mpp} = V_{max}/I_{max}$), was attached to the cell. So, the performance of devices can be recorded automatically with time to monitor the *J-V* curves. Because external load can be changed with the *J-V* results, the measured performance decay curves mean the performance decay behavior of cells under real operation. It is obvious that the results fully achieved the highest level of ISOS-L3.[31] The temperature of the cells is thermostatically controlled at room temperature 25 ℃ by temperature control equipment.

RESULTS AND DISCUSSION

Photovoltaic Performance of Cells with Glucose Modified ZnO ETL

Glucose molecule has five hydroxyl groups and one aldehyde group, which can be transferred to a six-member ring hemiacetal by a ring-chain tautomerism reaction (Fig. S1 in the electronic supplementary information, ESI). Therefore, it is expected that glucose should be able to passivate the surface defects of ZnO. Structure inverted PM6:Y6 solar cells using glucose modified ZnO (ZnO-Glu) as ETL were fabricated and tested (see Fig. 1a for the device structure). The reference cells using pristine ZnO were also invested for comparison. The current density-voltage (*J-V*) characteristics of the PSCs under

simulated AM 1.5G solar illumination are shown in Fig. 1(b). The photovoltaic performance data are listed in Table 1. As seen here, these control cells without glucose modification layer show an averaged PCE of 14.66% with a champion PCE of 14.77%. In contrast, the ZnO/Glu-based cells show a higher average and best PCE of 15.72% and 15.86%, respectively. The J_{SC} increased from 24.99 mA/cm^2 to 26.08 mA/cm^2, and the FF increased from 70.26% to 72.16% after surface modification with glucose, which are the main factors for the PCE improvement. Comparison of the cells' external quantum efficiency (EQE) spectra revealed that, although EQE improves over the entire absorption range of the cells, more significant improvement was found over 400–550 nm (Fig. 1c). The calculated J_{SC} from the integration of the EQE curves is 24.74 mA/cm^2 (pristine ZnO) and 26.21 mA/cm^2 (ZnO/Glu), which is a less than 5% mismatch than that of the J_{SC} value from the *J-V* curves. Fig. S2 in ESI shows the transmittance spectra and absorbance spectra of the glass/ZnO and glass/ZnO/Glu films prepared by the identical method for solar cells fabrication. As seen there, there is no obvious transmittance and absorbance

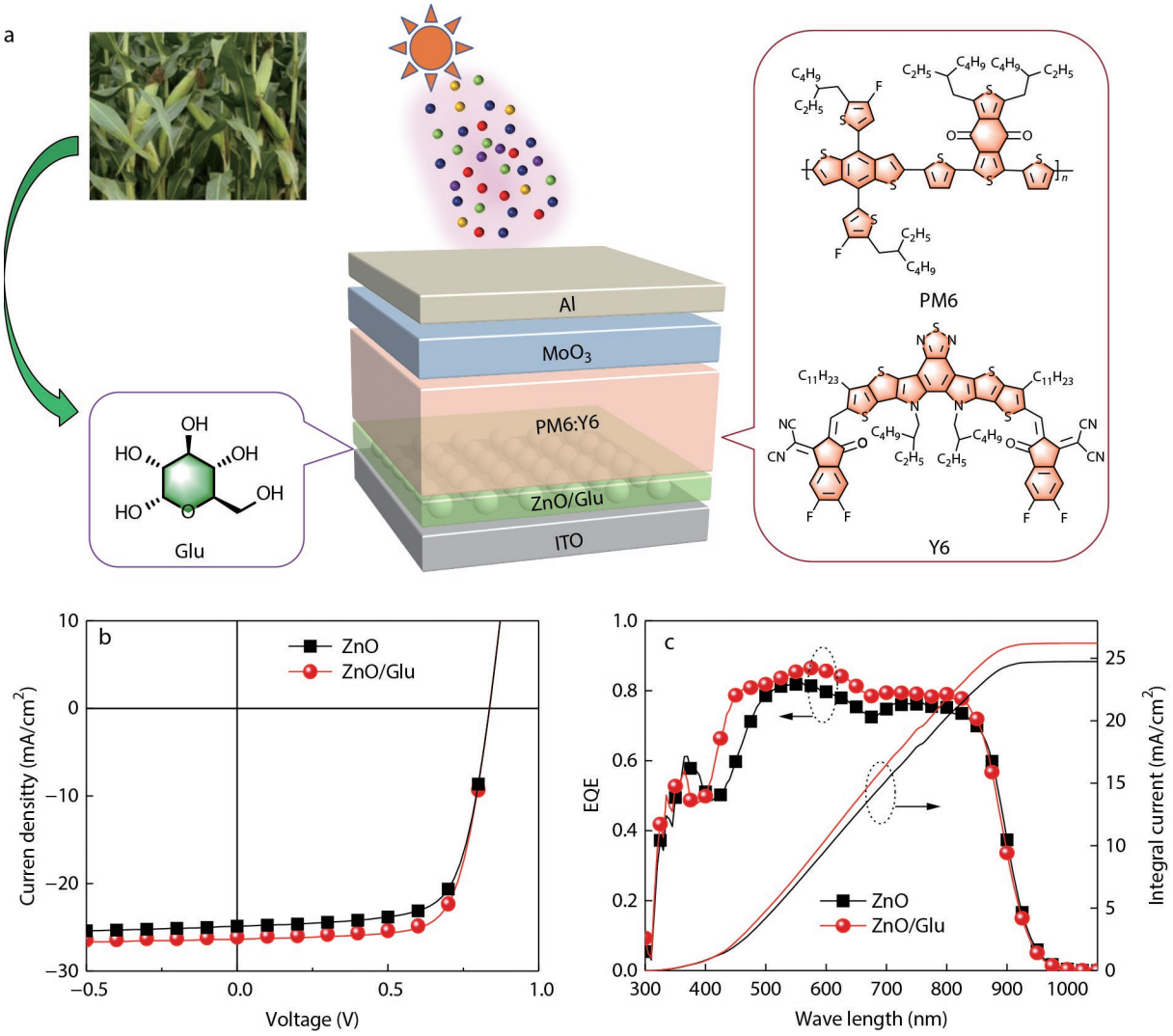

Fig. 1 (a) Solar cell device structure and molecule structures of active layer materials; (b) *J-V* curves and (c) EQE spectra of ZnO and ZnO/Glu cells.

Table 1 Performance parameters of the PM6:Y6, PM6:N3 and PM6:IT-4F inverted solar cells with pristine ZnO, and Glu-treated ZnO films as ETLs. [a]

ETL	ATL	V_{OC} (V)	J_{SC} (mA/cm^2)	FF (%)	PCE (%)	PCE_{max} [b] (%)
ZnO	PM6:Y6	0.836±0.002	24.99±0.01	70.26±0.00	14.66±0.114	14.77
ZnO/Glu	PM6:Y6	0.837±0.002	26.08±0.16	72.16±0.00	15.72±0.126	15.86
ZnO	PM6:N3	0.836±0.003	25.01±0.23	71.04±0.00	14.92±0.101	15.03
ZnO/Glu	PM6:N3	0.836±0.003	25.88±0.14	72.15±0.01	15.61±0.134	15.84
ZnO	PM6:IT-4F	0.829±0.003	19.13±0.04	70.27±0.00	11.14±0.012	11.16
ZnO/Glu	PM6:IT-4F	0.826±0.002	20.09±0.10	71.87±0.00	11.82±0.099	11.95

[a] Calculated from 8 individual devices; [b] Maximum PCE of the best cell.

https://doi.org/10.1007/s10118-022-2819-9

difference for these two films. Therefore, the increased EQE should not be attributed to the optical effect but to the improved charge injection and collection efficiency after coating the glucose layer. The more significant EQE enhancement at the short wavelength range implies the enhanced charge injection and collection efficiency mostly at the cathode side.

To further understand the interaction between glucose and ZnO, X-ray photoelectron spectroscopy (XPS) of ITO/ZnO and ITO/ZnO/Glu films were performed. The full XPS spectra are shown in Fig. S3 (in ESI), whereas the high-resolution C1s, Zn $2p_{3/2}$ and O1s are shown in Fig. 2. The C1s peaks for both films were measured to be broad, which can be divided into C=O (288.5 eV), C—O (286.4 eV) and C—C (284.8 eV). The proportion of C—O bonds on the surface of Glu-treated ZnO increased significantly from 24.72% to 47.36%. Since glucose is a polyhydroxy molecular, the increase of C—O ratio on surface of ZnO proves that a certain amount of glucose is attached to the ZnO surface. The XPS peaks of Zn $2p_{3/2}$ for the ZnO/Glu film were measured at 1021.43 eV, which is 0.45 eV shifted to the high binding energy when compared to that of the pristine ZnO film, suggesting that glucose molecules are intensively coordinated to Zn^{2+}.[32] The O1s core levels of ZnO film were deconvoluted into two different oxygen peaks at 529.61 and 531.20 eV (Fig. 2d), which can be assigned to oxygen in the oxide lattice (oxygen bonded to metal atoms) and surface-absorbed oxygen, such as hydroxy groups, respectively.[33] The position of the peaks of O 1s core levels for the ZnO/Glu films with 0.44 eV shifted to the high binding energy can also confirm the glucose molecules are intensively coordinated to Zn^{2+}. Besides, the proportion of the surface-absorbed oxygen in the glucose treated sample increased from 44.3% to 49.0%, indicating the intensive interaction of glucose with ZnO surface. PL was also characterized to clarify the passivation effect of the glucose and the results were shown in Fig. S4 (in ESI). The pristine ZnO film shows a broadband emission centered around 530 nm which has been well known as evidence of the presence of defect states (*e.g.*, oxygen vacancy) in ZnO.[34,35] After modified by glucose, the intensity of broadband defect emission was significantly reduced, confirming that the defect states were effectively recovered by glucose.

Influence of the Glucose Layer on the Interface between ZnO/PM6:Y6

Knowing that surface energy has a significant influence on the thin film formation on it, we measured the contact angle of water and CH_2I_2 on bare ZnO and ZnO/Glu film. As can be seen in Fig. 3(a), the contact angles of water on ZnO and ZnO/Glu films are 31.5° and 38.6°, respectively. In comparison, CH_2I_2 showed Cas of 51.0° and 40.9° on ZnO and ZnO/Glu, respectively. The surface free energy γ_s of ZnO and ZnO/Glu is then calculated to be 62.7 and 56.8 mN/m (Fig. S5 and Table S1 in ESI), respectively, according to the Owens-Wendt method.[36] These results indicate that glucose modification increases the hydrophobic feature of the ZnO/Glu film. Such an increased

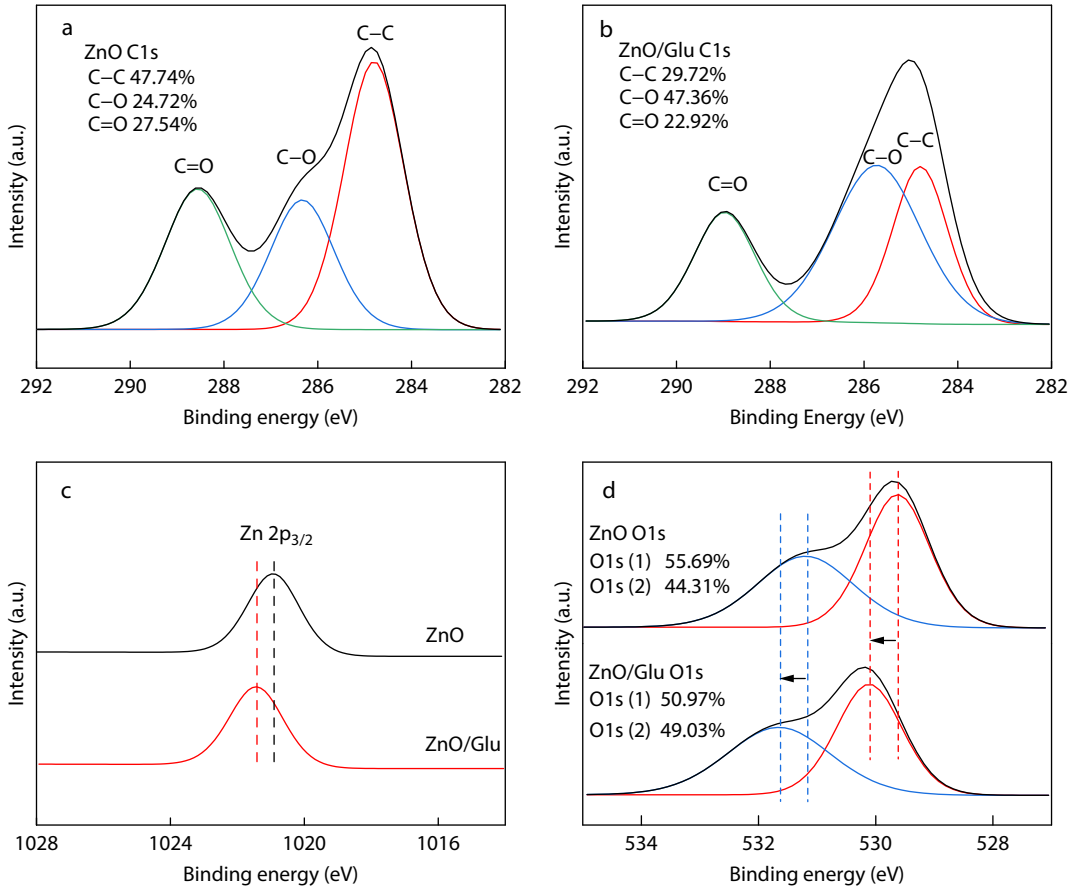

Fig. 2 C 1s XPS spectra of (a) ZnO and (b) ZnO/Glu; (c) XPS spectra of Zn $2p_{3/2}$ of ZnO and ZnO/Glu; (d) O1s XPS spectra of ZnO/Glu.

https://doi.org/10.1007/s10118-022-2819-9

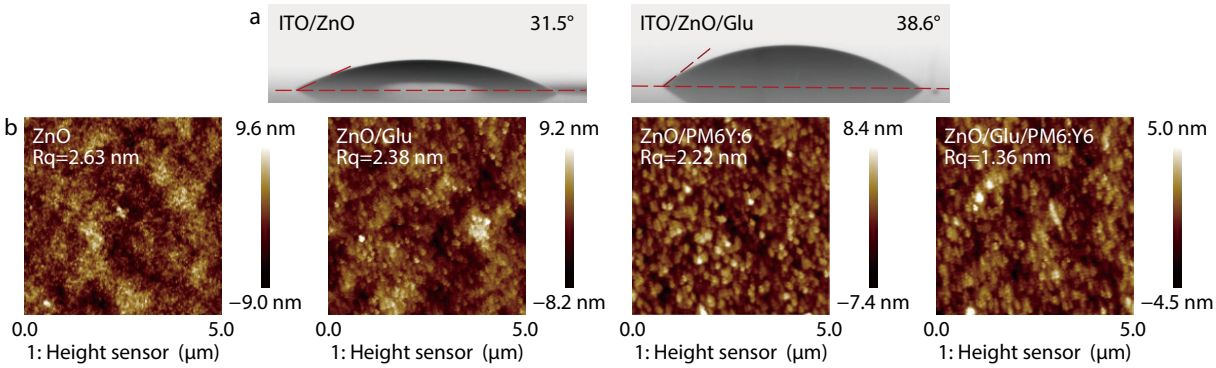

Fig. 3 (a) Contact angle of water on ITO/ZnO and ITO/ZnO/Glu surfaces; (b) AFM topographic images of ZnO, ZnO/Glu, ZnO/PM6:Y6 and ZnO/Glu/PM6:Y6 surfaces coated on ITO captured in tapping mode.

hydrophobic nature of the ZnO/Glu surface should be beneficial for the deposition of the photoactive layer,[37] since the organic semiconductors are usually dissolved in the organic solvent, which is more compatible with the hydrophobic organic active layer.

Surface morphologies of the ZnO and ZnO/Glu films were then characterized by atomic force microscopy (AFM). The topographic images are shown in Fig. 3(b), and the root mean square (RMS) roughness was measured to be 2.63 and 2.38 nm for the pristine ZnO and ZnO/Glu films, respectively, suggesting that glucose coating is able to smoothen the surface of ZnO film. The smoother surface of the ITO/ZnO/Glu film is beneficial for contacting the PM6:Y6 film. Fig. 3(b) also shows the surface morphology of ITO/ZnO/PM6:Y6 and ITO/ZnO/Glu/PM6:Y6 films. The RMS roughness of ZnO/BHJ and ZnO/Glu/PM6:Y6 was measured to be 2.22 and 1.36 nm, respectively. Again, surface modification of ZnO with glucose smoothened the surface morphology of the photoactive layer. Besides, the conductivities of ZnO and ZnO/Glu films were estimated by measuring the current-voltage (*I-V*) curves of the ITO/ETL/Al devices in the dark. As seen in Fig. S6 (in ESI) the ZnO/Glu ETL shows a typical diode characteristic, giving an improved conductivity than ZnO ETL. The improved conductivity can improve charge transport properties which will be beneficial to obtain reduced charge recombination at the interface. Then, ultraviolet photoelectron spectroscopy (UPS) measurements before and after the glucose modified were carried out (Fig. S7 in ESI). As seen here, the ZnO and ZnO/Glu exhibit a similar work function (WF) of 4.03 and 4.02 eV, respectively, indicating there is almost no change in the WF. Furthermore, the position of the valence band edge with respect to the surface Fermi level was determined by extrapolating the leading edge of the valence band photoemission spectra to the intersection with the background level to account for the finite resolution of the spectrometer (Fig. S7c in ESI). It is observed that the valence band edge of ZnO and ZnO/Glu are almost no change (3.22 and 3.18 eV respectively).

Figs. 4(a) and 4(b) show the dependence of V_{OC} and J_{SC} on the light intensity for these two cells. For an ideal p-n junction solar cell, V_{OC} can be calculated by the following Eq. (1):[38]

$$V_{OC} = \frac{nk_BT}{q}\ln\left(\frac{J_{ph}}{J_0} + 1\right) \quad (1)$$

where n is the ideality factor, k_B is the Boltzmann constant, T is the absolute temperature, q is the fundamental charge, J_{ph} is the photon-generated current, and J_0 is the dark-state reverse saturation current. J_{ph} as a photon-generated current is positively related to light intensity. Thus, V_{OC} is positively correlated with the logarithm of the light intensity, and the slope is equal to nK_BT/q. According to Fig. 4(a), the slopes of the ZnO and ZnO/Glu device were calculated to be $1.24k_BT/q$ and $1.21k_BT/q$, respectively. Compared to ZnO cell, a smaller ideality factor (n) for the ZnO/Glu cell indicates a lower trap assisted charge recombination (also named Shockley-Read-Hall (SRH) recombination) for the ZnO/Glu cell, which is beneficial for the charge transport and extraction.[39] Next, the inhibition of recombination was conducted through the dependence of J_{SC} on the light intensity. The relationship between J_{SC} and P_{light} can be described by $J_{sc} \propto P_{light}^{\alpha}$, where P_{light} is the light intensity and α is the exponential factor. Values of α for ZnO and ZnO/Glu devices are similar, 0.95 and 0.96, respectively, which indicate that Glu modification will slightly suppress the bimolecular recombination.[40] Then we measured the photocurrent density (J_{ph}) versus effective voltage (V_{eff}) curves to explore the enhancement of photovoltaic performance (Fig. 4c). J_{ph} is the difference between the current densities under light and dark. V_{eff} is the difference between applied voltage (V_{appl}) and V_0, where V_0 is the voltage when J_{ph} is zero.[41,42] We calculated the exciton dissociation probability by $P_{diss} = J_{ph}/J_{sat}$ where J_{sat} is the saturation photocurrent density when the value of V_{eff} was close to 2.0 V. Under short-circuit conditions, P_{diss} of the ZnO/Glu device is 97.9%, obviously higher than that of ZnO with 95.7% (Table S2 in ESI), demonstrating a more effective exciton dissociation and charge collection for the ZnO/Glu device. Besides, dark *J-V* characteristic was also tested, which provided some important information for the changes of these interface layers. As seen in Fig. S8 (in ESI) that the leakage current of ZnO/Glu layer devices is reduced in the forward-biased and reverse-biased regions, while the ZnO-based devices show higher leakage current than that of Glu modified one, indicating that the introduction of Glu can effectively optimize the charge injection process.[43] In the high voltage regime, the series resistance depends on the dark current. Fig. 4(d) gives the plots of dV/dJ versus $(J - J_{SC})^{-1}$ and the linear fitting curves according to Eq. (2):[44]

$$\frac{dV}{dJ} = \frac{nk_BT}{q}\left(\frac{1}{J - J_{SC}}\right) + R_S \quad (2)$$

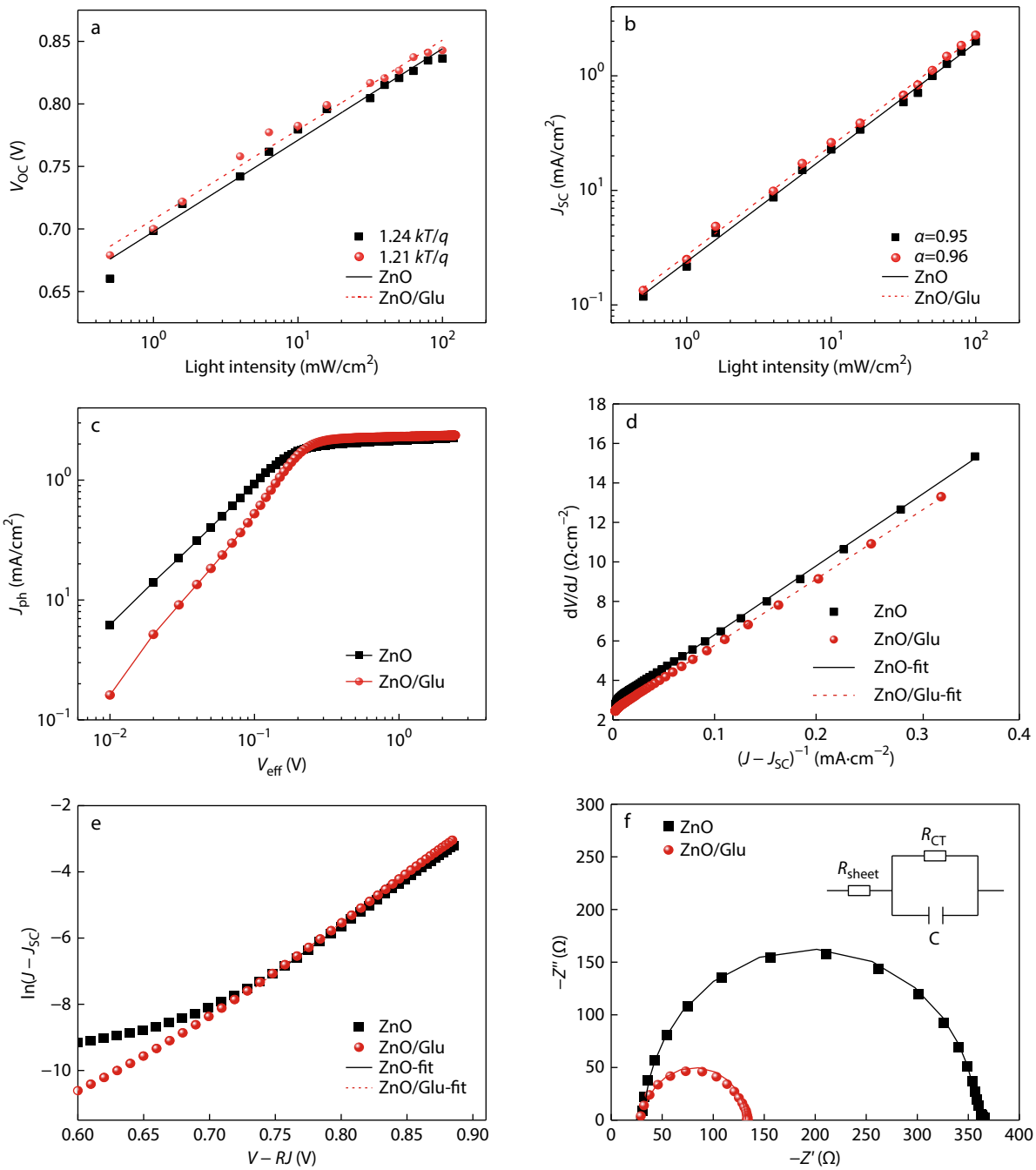

Fig. 4 (a) V_{OC} and (b) J_{SC} versus light intensity plot; (c) Photocurrent density versus effective voltage curves of PM6:Y6 solar cells with ZnO, ZnO/Glu as ETL; (d) Plots of dV/dJ versus $(J - J_{SC})^{-1}$ and the linear fitting curves; (e) Plots of ln($J - J_{SC}$) against $V - RJ$ and the linear fitting curves; (f) Nyquist plot of the devices based on ZnO and ZnO/Glu as ETL and the equivalent-circuit model employed for EIS fitting.

The ideality factor (n) and series resistance (R_S) of the cell are derived from the slope and intercept of the linear fitting results, as shown in Table S3 (in ESI). For ZnO device, the n is 1.35 and the R_S is 2.84 ohm/cm^2, while for ZnO/Glu device n is 1.30 and the R_S is 2.43 ohm/cm^2. The smaller ideality factor (n) for the ZnO/Glu cell indicates a lower SRH recombination which is consistent with the light intensity dependence result. Besides, the higher FF of ZnO/Glu device can be attributed to the smaller R_S. Fig. 4(e) gives the plots of ln($J - J_{SC}$) versus $V - JR_S$ and the linear fitting curves according to Eq. (3):[44]

$$\ln(J - J_{SC}) = \frac{q(V - JR_S)}{nk_BT} + \ln J_0 \quad (3)$$

The ideality factor and reverse saturated current density are also derived from the linear fitting results, as in Table S3 (in ESI). For ZnO and ZnO/Glu devices, n are 1.36 and 1.31, respectively, which is very close to that derived from plots of dV/dJ versus $(J - J_{SC})^{-1}$ in Fig. 4(d). Compared to the ZnO device, the J_0 of the ZnO/Glu device decreased from 4.06×10^{-13} mA/cm^2 to 1.74×10^{-13} mA/cm^2, which means the lower recombination. Therefore, the electron transport and

https://doi.org/10.1007/s10118-022-2819-9

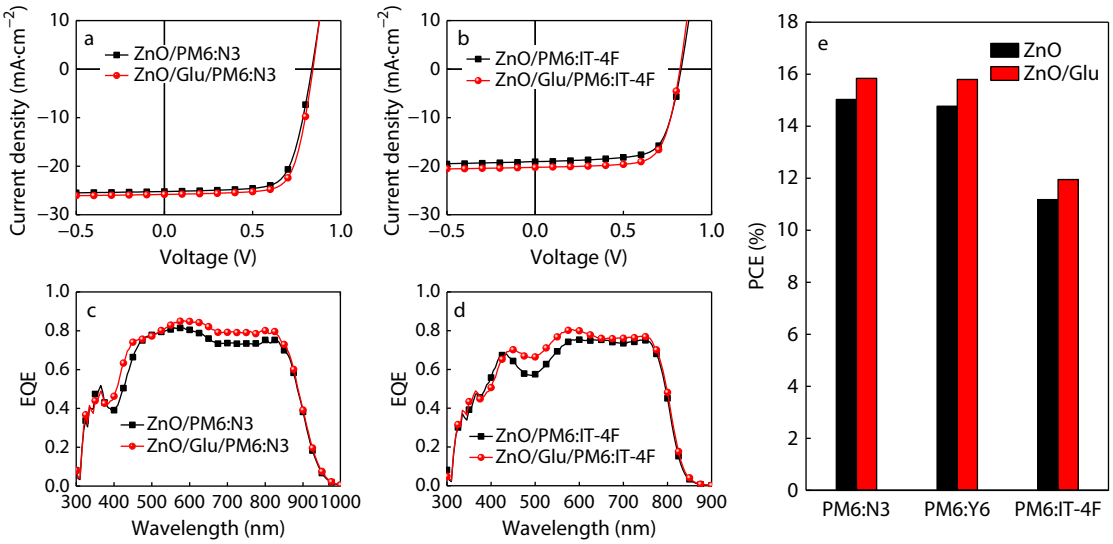

Fig. 5 Current density versus voltage (*J-V*) characteristics of (a) PM6:N3, (b) PM6:IT-4F solar cells under AM1.5G solar irradiation based on ZnO and ZnO/Glu electron transport layers; EQE characteristics of (c) PM6:N3, (d) PM6:IT-4F solar cells; (e) Comparison of PCEs in different BHJ systems with and without Glu layers.

collection were enhanced at the electrode and active layer interface.[45] As shown in the inserted image of Fig. 4(f), impedance spectra of ZnO, ZnO/Glu were fitted with the equivalent circuit model that comprised of two resistances R_{SH} (sheet resistance), R_{CT} (charge transport resistance) and one capacitances (*C*). The R_{SH} is mainly determined by the electrodes and the R_{CT} is related to the active layer/electrode interfaces and the active layers.[46] The fitting parameters are summarized in Table S4 (in ESI). For the pristine ZnO device, R_{SH}, R_{CT}, *C* were 32.9 ohm, 330.0 ohm and 1.6×10^{-9} F, respectively. Compared with the pristine ZnO device, the devices with the Glu-treated ZnO ETL displayed similar R_{SH} (32.1 ohm) but smaller R_{CT} (99.7 ohm) indicating the improved electron transfer and collection in these OSCs. This reveals that glucose layer has played a decisive role to improve the charge transfer and collection, which is in line with the reduced properties of the dark *J-V* characteristics. In general, the improvement in J_{SC} and FF we observed in the ZnO/Glu device should be attributed to the improved electron transfer and collection as well as lower trap assisted charge recombination, which may be related to improved interface compatibility, including smaller γ_s and RMS.[47,48]

Generality of Glucose Passivation in PSCs

To check the generality of glucose passivation of ZnO surface in improving device performance, we fabricated and tested the photovoltaic performance of polymer solar cells using PM6 as the polymer donor and N3/IT-4F as the electron acceptor (Fig. S9 in ESI for the chemical structure of N3/IT-4F). The *J-V* curves and EQE spectra of the cells are shown in Fig. 5, and the device performance data are summarized in Table 1. The control device based on the neat ZnO electron transport layer for PM6:N3 BHJ layers yields an average PCE of 14.92 (the maximum of 15.03%), consistent with the reported value in the literature.[49] As expected, the device with ZnO/Glu shows an enhancement in J_{SC} (from 25.01 mA/cm^2 to 25.88 mA/cm^2) and FF (from 71.04% to 72.15%), and the resultant PCE reached 15.61% (15.84%). Similarly, for the PM6:IT-4F cells, the use of ZnO/Glu ETL showed an improved PCE of 11.82% (11.95%) when compared to the corresponding cells with ZnO ETL, where J_{SC} of 19.13 mA/cm^2, a V_{OC} of 0.829 V and a FF of 70.27% while the glucose containing device exhibited an increased J_{SC} from 19.13 mA/cm^2 to 20.09 mA/cm^2 and FF from 70.27% to 71.87% (Table 1). The higher J_{SC} and FF can be correlated to the interfacial passivation effect of glucose, which originated from the hydrophobic and smooth surface of ZnO/Glu, leading to efficient electron extraction and better contact with the photoactive layer, as mentioned above. We can also observe a clear enhancement in the PCE of different BHJ systems with and without the Glu layer, as shown in Fig. 4(e).

Stability Improvement of the Cells by Glucose Modification

We then compared the stability of the cells under light illumination. All these cells were aged inside the glovebox (with H_2O<10 ppm, O_2<10 ppm) with continuous light illumination. Fig. 6(a) depicts the PCE decay curves of these cells. The complete decay traces of the photovoltaic performance of these cells are shown in Fig. S10 in ESI. As seen here, the ZnO/PM6:Y6 cells under light illumination were reduced to 31% of their initial values over 500 h (60% for V_{OC}, 63% for J_{SC} and 72% for FF), while the PCE of the ZnO/Glu based cells still maintained 92% of their initial values after aged for 1250 h (98% for V_{OC}, 99% for J_{SC} and 95% for FF), indicating excellent stability for this cell. Especially, there is almost no J_{SC} decay measured of the cells, indicating that the interfacial decomposition of NFA on ZnO surface was dramatically reduced with the surface passivation of glucose. To quantitatively analyze the degradation processes of cells, the PCE decays were numerically fitted to a stretched exponential model according to the Eq. (4):[26,50]

$$\mathrm{PCE}(t) = \mathrm{PCE}(\infty) + \alpha \times \exp\left(-\frac{t}{\tau}\right)^{\beta} \quad (4)$$

where τ, α, and PCE(∞) represent the mean lifetime, pre-exponential factor (degradation amplitudes), and the intercept (the saturated PCE over a long time aging), respectively. The stretching exponent β is in the range $0<\beta\leq1$, which indicates the complexity of the decay process. As seen in Fig. S11 and Table

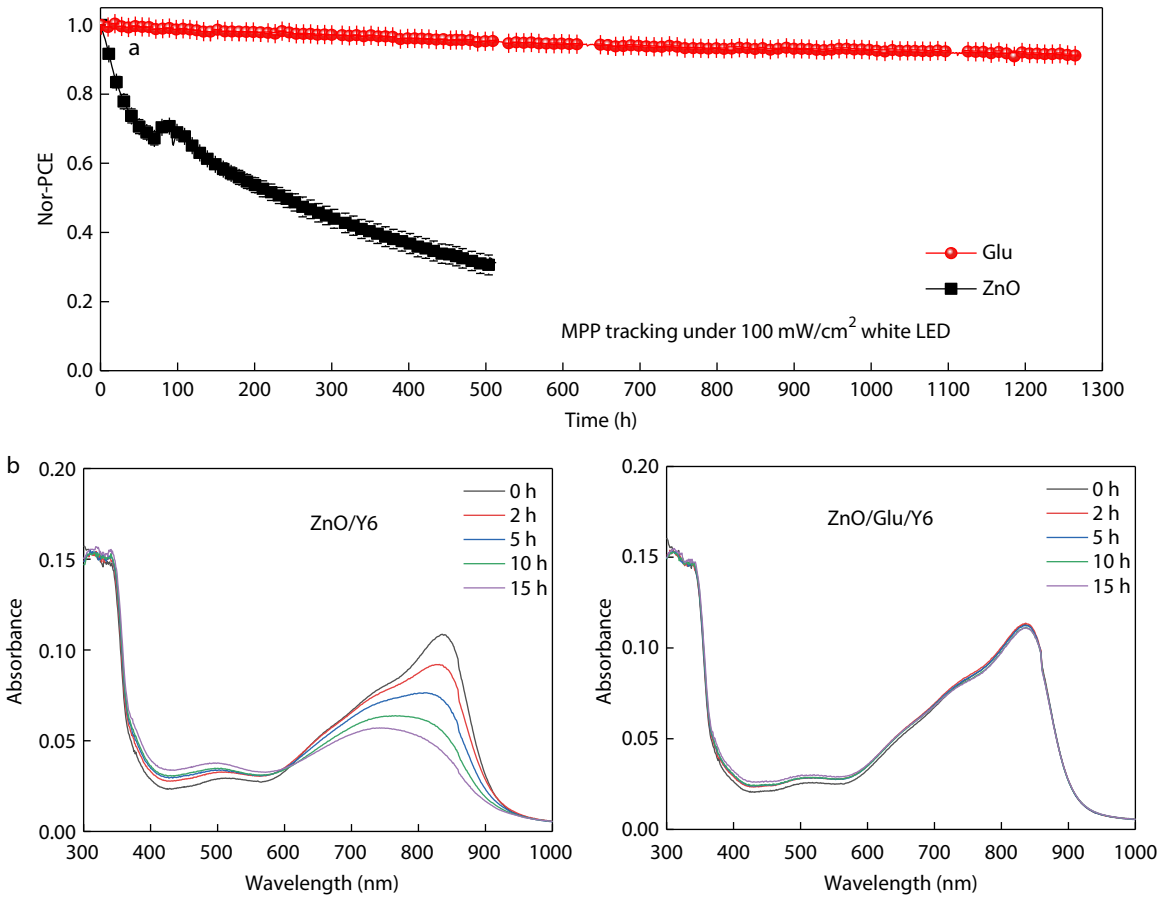

Fig. 6 (a) Evolution of device performance of ZnO/PM6:Y6 and ZnO/Glu/PM6:Y6 cells; (b) UV-Vis absorption changes of ZnO/Y6 and ZnO/Glu/Y6 under white light illumination.

S5 (in ESI), the ZnO devices have a mean lifetime (τ) of 224 h and a PCE(∞) of 0.25. As for ZnO/Glu device, the mean lifetime is 973 h which is higher than ZnO cells, suggesting much higher stability for the ZnO/Glu based cell, whereas the high PCE(∞) of 0.88 suggests that the cell should keep 88% of its initial efficiency over long time aging if the decay of the cell following an exponential decay. After glucose modification, the slight decays of V_{OC} and FF were also measured for these cells, which may be attributed to the interfacial degradation at the polymer/MoO_3 interface.[51,52] To further prove that surface treatment of the ZnO layer improves the stability of the devices by suppressing the interfacial photochemical reaction, we then check the photon bleaching off thin films with a structure of ITO/ZnO/Y6 and ITO/ZnO/Glu/Y6. The UV-Vis absorption spectra of films were then recorded, and the results are shown in Fig. 6(b). Compared with the ZnO/Y6 film, the absorption changes in ZnO/Glu/Y6 film have slowed down clearly after the surface treatment, corresponding well to the device stability improvement results. In our previous work, photon-generated hydroxyl radical on the ZnO surface is the chemically reactive species that causes the breaking of the C=C bonds of NFAs has been proved.[22,26] Due to the polyhydroxylation of glucose, we believe that the hydrogen atoms of glucose can combine with the hydroxyl groups on the surface of ZnO to inhibit the generation of hydroxyl radicals in ZnO. Besides, the stabilities of the cells in the air and dark environment without encapsulation were also compared. All these cells were stored in an air environment (relative humidity 30%–35%, temperature 20–25 °C) without illumination. The complete decay traces of the photovoltaic performance of these cells are shown in Fig. S12 in ESI. As seen here, the ZnO/PM6:Y6 cells were reduced to 34% of their initial PCE over 45 h (51% for V_{OC}, 95% for J_{SC} and 69% for FF). On the contrary, the PCE of the ZnO/Glu based cells show better stability maintaining 76% of their initial values (86% for V_{OC}, 98% for J_{SC} and 89% for FF) over 45 h, which should be attributed to the passivation of glucose.

CONCLUSIONS

In summary, environmentally friendly glucose was used as a modified layer of ZnO to simultaneously improve the efficiency and stability of high-performance polymer:non-fullerene solar cells. X-ray photoelectron spectroscopy (XPS) measurements reveal that glucose is successfully attached to ZnO and the intensive interaction passivate the oxygen vacancies. Under the optimal conditions, we improved PCEs from 14.77% to 15.86% based on PM6:Y6 BHJs, due to a concurrently increased short-circuit current and fill factor. The homogeneous surface morphology with relatively lower hydrophilicity and the smoother surface of the ITO/ZnO/Glu film are beneficial to contact the active layer at the interface. The dependence of V_{OC} and J_{SC} on the light intensity and dark *J-V* reveal that the modification of glucose on ZnO can effectively promote exciton dissociation and play a key role in inhibiting charge

https://doi.org/10.1007/s10118-022-2819-9

recombination for improved photovoltaic performances. UV-Vis absorption reveal Glu modification can significantly inhibit the photodegradation of Y6 acceptors, resulting in a significant improvement in the stability of the device. Finally, the Glu-modified device still maintains 92% of its initial PCE after being aged for 1250 h. The application of natural interface materials in this work brings hope for the commercial application of organic solar cells and provides new ideas for the development of new interface materials.

NOTES

The authors declare no competing financial interest.

Electronic Supplementary Information

Electronic supplementary information (ESI) is available free of charge in the online version of this article at http://doi.org/10.1007/s10118-022-2819-9.

ACKNOWLEDGMENTS

This work was financially supported by the National Natural Science Foundation of China (No. 22075315), the Chinese Academy of Science (Nos. YJKYYQ20180029 and GJHZ2092-019) and the Youth Innovation Promotion Association, CAS (No. 2019317).

REFERENCES

1 Li, Y.; Xu, G.; Cui, C.; Li, Y. Flexible and semitransparent organic solar cells. *Adv. Energy Mater.* **2018**, *8*, 1701791.
2 Zhang, K.; Hu, Z.; Sun, C.; Wu, Z.; Huang, F.; Cao, Y. Toward solution-processed high-performance polymer solar cells: from material design to device engineering. *Chem. Mater.* **2017**, *29*, 141–148.
3 Kang, H.; Kim, G.; Kim, J.; Kwon, S.; Kim, H.; Lee, K. Bulk-heterojunction organic solar cells: five core technologies for their commercialization. *Adv. Mater.* **2016**, *28*, 7821–7861.
4 Cui, Y.; Xu, Y.; Yao, H.; Bi, P.; Hong, L.; Zhang, J.; Zu, Y.; Zhang, T.; Qin, J.; Ren, J.; Chen, Z.; He, C.; Hao, X.; Wei, Z.; Hou, J. Single-junction organic photovoltaic cell with 19% efficiency. *Adv. Mater.* **2021**, *33*, 2102420.
5 An, C.; Zheng, Z.; Hou, J. Recent progress in wide bandgap conjugated polymer donors for high-performance nonfullerene organic photovoltaics. *Chem. Commun.* **2020**, *56*, 4750–4760.
6 Fu, H.; Wang, Z.; Sun, Y. Polymer donors for high-performance non-fullerene organic solar cells. *Angew. Chem. Int. Ed.* **2019**, *58*, 4442–4453.
7 Sun, H.; Chen, F.; Chen, Z. K. Recent progress on non-fullerene acceptors for organic photovoltaics. *Mater. Today* **2019**, *24*, 94–118.
8 Zhang, G.; Zhao, J.; Chow, P. C.; Jiang, K.; Zhang, J.; Zhu, Z.; Zhang, J.; Huang, F.; Yan, H. Nonfullerene acceptor molecules for bulk heterojunction organic solar cells. *Chem. Rev.* **2018**, *118*, 3447–3507.
9 Cheng, P.; Li, G.; Zhan, X.; Yang, Y. Next-generation organic photovoltaics based on non-fullerene acceptors. *Nat. Photon.* **2018**, *12*, 131–142.
10 Liu, Y.; Liu, B.; Ma, C.-Q.; Huang, F.; Feng, G.; Chen, H.; Hou, J.; Yan, L.; Wei, Q.; Luo, Q.; Bao, Q.; Ma, W.; Liu, W.; Li, W.; Wan, X.; Hu, X.; Han, Y.; Li, Y.; Zhou, Y.; Zou, Y.; Chen, Y.; Li, Y.; Chen, Y.; Tang, Z.; Hu, Z.; Zhang, Z. G.; Bo, Z. Recent progress in organic solar cells (Part I material science). *Sci. China Chem.* **2022**, *65*, 224–268.
11 Zhang, M.; Guo, X.; Ma, W.; Ade, H.; Hou, J. A large-bandgap conjugated polymer for versatile photovoltaic applications with high performance. *Adv. Mater.* **2015**, *27*, 4655–4660.
12 Yuan, J.; Zhang, Y.; Zhou, L.; Zhang, G.; Yip, H. L.; Lau, T. K.; Lu, X.; Zhu, C.; Peng, H.; Johnson, P. A.; Leclerc, M.; Cao, Y.; Ulanski, J.; Li, Y.; Zou, Y. Single-junction organic solar cell with over 15% efficiency using fused-ring acceptor with electron-deficient core. *Joule* **2019**, *3*, 1140–1151.
13 Chen, H.; Zhang, R.; Chen, X.; Zeng, G.; Kobera, L.; Abbrent, S.; Zhang, B.; Chen, W.; Xu, G.; Oh, J. A guest-assisted molecular-organization approach for >17% efficiency organic solar cells using environmentally friendly solvents. *Nat. Energy* **2021**, *6*, 1045–1053.
14 Zhang, M.; Zhu, L.; Zhou, G.; Hao, T.; Qiu, C.; Zhao, Z.; Hu, Q.; Larson, B. W.; Zhu, H.; Ma, Z.; Tang, Z.; Feng, W.; Zhang, Y.; Russell, T. P.; Liu, F. Single-layered organic photovoltaics with double cascading charge transport pathways: 18% efficiencies. *Nat. Commun.* **2021**, *12*, 309.
15 Li, G.; Chu, C.-W.; Shrotriya, V.; Huang, J.; Yang, Y. Efficient inverted polymer solar cells. *Appl. Phys. Lett.* **2006**, *88*, 253503.
16 Zhang, H.; Li, Y.; Zhang, X.; Zhang, Y.; Zhou, H. Role of interface properties in organic solar cells: from substrate engineering to bulk-heterojunction interfacial morphology. *Mater. Chem. Front.* **2020**, *4*, 2863–2880.
17 Tran, H. N.; Park, S.; Wibowo, F. T. A.; Krishna, N. V.; Kang, J. H.; Seo, J. H.; Nguyen-Phu, H.; Jang, S. Y.; Cho, S. 17% Non-fullerene organic solar cells with annealing-free aqueous MoOx. *Adv. Sci.* **2020,** *7*, 2002395.
18 Lee, B. R.; Jung, E. D.; Nam, Y. S.; Jung, M.; Park, J. S.; Lee, S.; Choi, H.; Ko, S. J.; Shin, N. R.; Kim, Y. K. Amine-based polar solvent treatment for highly efficient inverted polymer solar cells. *Adv. Mater.* **2014**, *26*, 494–500.
19 Liang, Z.; Zhang, Q.; Jiang, L.; Cao, G. ZnO cathode buffer layers for inverted polymer solar cells. *Energy Environ. Sci.* **2015**, *8*, 3442–3476.
20 Sekine, N.; Chou, C.-H.; Kwan, W. L.; Yang, Y. ZnO nano-ridge structure and its application in inverted polymer solar cell. *Org. Electron.* **2009**, *10*, 1473–1477.
21 Li, D.; Qin, W.; Zhang, S.; Liu, D.; Yu, Z.; Mao, J.; Wu, L.; Yang, L.; Yin, S. Effect of UV-ozone process on the ZnO interlayer in the inverted organic solar cells. *RSC advances* **2017**, *7*, 6040–6045.
22 Liu, B.; Han, Y.; Li, Z.; Gu, H.; Yan, L.; Lin, Y.; Luo, Q.; Yang, S.; Ma, C. Q. Visible light-induced degradation of inverted polymer: nonfullerene acceptor solar cells: initiated by the light absorption of ZnO layer. *Sol. RRL* **2021**, *5*, 2000638.
23 Bao, Q.; Liu, X.; Xia, Y.; Gao, F.; Kauffmann, L.-D.; Margeat, O.; Ackermann, J.; Fahlman, M. Effects of ultraviolet soaking on surface electronic structures of solution processed ZnO nanoparticle films in polymer solar cells. *J. Mater. Chem. A* **2014**, *2*, 17676–17682.
24 Wang, Y.; Yan, L.; Ji, G.; Wang, C.; Gu, H.; Luo, Q.; Chen, Q.; Chen, L.; Yang, Y.; Ma, C. Q. Synthesis of N,S-doped carbon quantum dots for use in organic solar cells as the ZnO modifier to eliminate the light-soaking effect. *ACS Appl. Mater. Interfaces* **2018**, *11*, 2243–2253.
25 Hu, L.; Jiang, Y.; Sun, L.; Xie, C.; Qin, F.; Wang, W.; Zhou, Y. Significant enhancement of illumination stability of nonfullerene organic solar cells *via* an aqueous polyethylenimine modification. *J. Phys. Chem. Lett.* **2021**, *12*, 2607–2614.
26 Liu, B.; Su, X.; Lin, Y.; Li, Z.; Yan, L.; Han, Y.; Luo, Q.; Fang, J.; Yang, S.; Tan, H. Simultaneously achieving highly efficient and stable polymer: non-fullerene solar cells enabled by molecular structure

optimization and surface passivation. *Adv. Sci.* **2022**, *9*, 2104588.
27 Bai, S.; Jin, Y.; Liang, X.; Ye, Z.; Wu, Z.; Sun, B.; Ma, Z.; Tang, Z.; Wang, J.; Würfel, U. Ethanedithiol treatment of solution-processed ZnO thin films: controlling the intragap states of electron transporting interlayers for efficient and stable inverted organic photovoltaics. *Adv. Energy Mater.* **2015**, *5*, 1401606.
28 Han, Y.; Dong, H.; Pan, W.; Liu, B.; Chen, X.; Huang, R.; Li, Z.; Li, F.; Luo, Q.; Zhang, J. An Efficiency of 16.46% and a T 80 lifetime of over 4000 h for the PM6:Y6 inverted organic solar cells enabled by surface acid treatment of the zinc oxide electron transporting layer. *ACS Appl. Mater. Interfaces* **2021**, *13*, 17869–17881.
29 Lin, P. C.; Wong, Y. T.; Su, Y. A.; Chen, W. C.; Chueh, C. C. Interlayer modification using eco-friendly glucose-based natural polymers in polymer solar cells. *ACS Sustain. Chem. Eng.* **2018**, *6*, 14621–14630.
30 Qian, L.; Zheng, Y.; Choudhury, K. R.; Bera, D.; So, F.; Xue, J.; Holloway, P. H. Electroluminescence from light-emitting polymer/ZnO nanoparticle heterojunctions at sub-bandgap voltages. *Nano Today* **2010**, *5*, 384–389.
31 Reese, M. O.; Gevorgyan, S. A.; Jørgensen, M.; Bundgaard, E.; Kurtz, S. R.; Ginley, D. S.; Olson, D. C.; Lloyd, M. T.; Morvillo, P.; Katz, E. A. Consensus stability testing protocols for organic photovoltaic materials and devices. *Sol. Energ. Mat. Sol. C.* **2011**, *95*, 1253–1267.
32 Polydorou, E.; Zeniou, A.; Tsikritzis, D.; Soultati, A.; Sakellis, I.; Gardelis, S.; Papadopoulos, T. A.; Briscoe, J.; Palilis, L. C.; Kennou, S.; Gogolides, E.; Argitis, P.; Davazoglou, D.; Vasilopoulou, M. Surface passivation effect by fluorine plasma treatment on ZnO for efficiency and lifetime improvement of inverted polymer solar cells. *J. Mater. Chem. A* **2016**, *4*, 11844–11858.
33 Jeong, S.; Ha, Y. G.; Moon, J.; Facchetti, A.; Marks, T. J. Role of gallium doping in dramatically lowering amorphous-oxide processing temperatures for solution-derived indium zinc oxide thin-film transistors. *Adv. Mater.* **2010**, *22*, 1346–1350.
34 Ischenko, V.; Polarz, S.; Grote, D.; Stavarache, V.; Fink, K.; Driess, M. Zinc oxide nanoparticles with defects. *Adv. Funct. Mater.* **2005**, *15*, 1945–1954.
35 Janotti, A.; Van de Walle, C. G. Native point defects in ZnO. *Phys. Rev. B* **2007**, *76*, 165202.
36 Comyn, J. Contact angles and adhesive bonding. *Int. J. Adhes. Adhesiv.* **1992**, *12*, 145–149.
37 Liu, C.; Zhang, L.; Xiao, L.; Peng, X.; Cao, Y. Doping ZnO with water/alcohol-soluble small molecules as electron transport layers for inverted polymer solar cells. *ACS Appl. Mater. Interfaces* **2016**, *8*, 28225–28230.
38 Wetzelaer, G.; Kuik, M.; Lenes, M.; Blom, P. Origin of the dark-current ideality factor in polymer: fullerene bulk heterojunction solar cells. *Appl. Phys. Lett.* **2011**, *99*, 153506.
39 Cowan, S. R.; Wang, J.; Yi, J.; Lee, Y.-J.; Olson, D. C.; Hsu, J. W. Intensity and wavelength dependence of bimolecular recombination in P3HT:PCBM solar cells: a white-light biased external quantum efficiency study. *J. Appl. Phys.* **2013**, *113*, 154504.
40 Yu, R.; Wei, X.; Wu, G.; Zhang, T.; Gong, Y.; Zhao, B.; Hou, J.; Yang, C.; Tan, Z. A. Efficient interface modification *via* multi-site coordination for improved efficiency and stability in organic solar cells. *Energy Environ. Sci.* **2022**, *15*, 822–829.
41 Mihailetchi, V. D.; Koster, L. J. A.; Hummelen, J. C.; Blom, P. W. M. Photocurrent generation in polymer-fullerene bulk heterojunctions. *Phys. Rev. Lett.* **2004**, *93*, 216601.
42 Blom, P. W. M.; Mihailetchi, V. D.; Koster, L. J. A.; Markov, D. E. Device physics of polymer:fullerene bulk heterojunction solar cells. *Adv. Mater.* **2007**, *19*, 1551–1566.
43 Gao, Y.; Yip, H.-L.; Hau, S. K.; O'Malley, K. M.; Cho, N. C.; Chen, H.; Jen, A. K. Y. Anode modification of inverted polymer solar cells using graphene oxide. *Appl. Phys. Lett.* **2010**, *97*, 251.
44 Shi, J.; Dong, J.; Lv, S.; Xu, Y.; Zhu, L.; Xiao, J.; Xu, X.; Wu, H.; Li, D.; Luo, Y.; Meng, Q. Hole-conductor-free perovskite organic lead iodide heterojunction thin-film solar cells: high efficiency and junction property. *Appl. Phys. Lett.* **2014**, *104*, 063901.
45 Chen, X.; Zhu, B.; Kan, B.; Gao, K.; Peng, X.; Cao, Y. Cathode interlayer-free organic solar cells with enhanced device performance upon alcohol treatment. *J. Mater. Chem. C* **2019**, *7*, 7947–7952.
46 Kim, J. S.; Chung, W. S.; Kim, K.; Kim, D. Y.; Paeng, K. J.; Jo, S. M.; Jang, S. Y. Performance optimization of polymer solar cells using electrostatically sprayed photoactive layers. *Adv. Funct. Mater.* **2010**, *20*, 3538–3546.
47 Yin, Z.; Zheng, Q.; Chen, S. C.; Cai, D.; Ma, Y. Controllable ZnMgO electron-transporting layers for long-term stable organic solar cells with 8. 06% efficiency after one-year storage. *Adv. Energy Mater.* **2016**, *6*, 1501493.
48 Seitkhan, A.; Neophytou, M.; Kirkus, M.; Abou-Hamad, E.; Hedhili, M. N.; Yengel, E.; Firdaus, Y.; Faber, H.; Lin, Y.; Tsetseris, L. Use of the phen-NaDPO:Sn (SCN)2 blend as electron transport layer results to consistent efficiency improvements in organic and hybrid perovskite solar cells. *Adv. Funct. Mater.* **2019**, *29*, 1905810.
49 Jiang, K.; Wei, Q.; Lai, J. Y. L.; Peng, Z.; Kim, H. K.; Yuan, J.; Ye, L.; Ade, H.; Zou, Y.; Yan, H. Alkyl chain tuning of small molecule acceptors for efficient organic solar cells. *Joule* **2019**, *3*, 3020–3033.
50 Johnston, D. Stretched exponential relaxation arising from a continuous sum of exponential decays. *Phys. Rev. B* **2006**, *74*, 184430.
51 Doumon, N. Y.; Houard, F. V.; Dong, J.; Yao, H.; Portale, G.; Hou, J.; Koster, L. J. A. Energy level modulation of ITIC derivatives: effects on the photodegradation of conventional and inverted organic solar cells. *Org. Electron.* **2019**, *69*, 255–262.
52 Gu, H.; Yan, L.; Saxena, S.; Shi, X.; Zhang, X.; Li, Z.; Luo, Q.; Zhou, H.; Yang, Y.; Liu, X.; Wong, W. W. H.; Ma, C. Q. Revealing the interfacial photoreduction of MoO_3 with P3HT from the molecular weight-dependent "burn-in" degradation of P3HT:PC61BM solar cells. *ACS Appl. Energy Mater.* **2020**, *3*, 9714–9723.

https://doi.org/10.1007/s10118-022-2819-9